European Journal of Immunology

WILEY-VCH

European Journal of Immunology
Basic • Clinical • Translational

RESEARCH ARTICLE

Tumor Immunology

ICAM-1 Is Overexpressed by Cancers and Negatively Impacts Antibody-Based Therapies Including Antibody–Drug Conjugates

J. Bradford Kline | Luigi Grasso | Nicholas C. Nicolaides

Navrogen Inc., 1837 University Circle, Cheyney, Pennsylvania, USA

Correspondence: Nicholas C. Nicolaides (nick@navrogen.com)

Received: 28 October 2024 | **Revised:** 11 February 2025 | **Accepted:** 14 February 2025

Funding: The authors received no specific funding for this work.

Keywords: antibody therapeutics | antibody–drug conjugates | ICAM-1 | immune effector | immunosuppression

ABSTRACT

Humoral immunity utilizes antibodies and immune effector cells to mediate dysregulated cancer cell killing. These mechanisms are referred to as Humoral Immuno-Oncology (HIO). HIO immunosuppression is mediated by tumor-produced proteins called HIO factors. Using a combination of patient serum analysis and literature searches, we screened a number of samples to determine if they suppressed HIO. Herein, we identified that ICAM-1 (intercellular adhesion molecule 1) can bind IgG1-type antibodies and suppress their immune effector activity. Through a series of mutagenesis, we identified a unique motif within the IgG1CH3 domain essential for ICAM-1 binding, which inhibits antibody-dependent cellular cytotoxicity and complement-dependent cytotoxicity. Conservative amino acid substitutions within the CH3 domain were able to abrogate ICAM-1 binding and overcome ICAM-1 mediated immune effector suppression. Additionally, isogenic tumor cell lines with silenced ICAM-1 expression were more susceptible to antibody–drug conjugate (ADCs) cytotoxicity than parental cells. This effect appeared to correlate with membrane ICAM-1 binding to the IgG1 component that reduced ADC internalization, a function important for maximal target cell killing. These findings highlight a novel mechanism by which tumors can suppress the host's immune system for survival and offer new concepts for engineering antibody-based therapeutics that are refractory to ICAM-1 immunosuppression.

1 | Introduction

Humoral immunity is a mechanism by which vertebrates surveil and defend against dysregulated host cells via antibody-mediated killing. In cancer biology, immune checkpoint inhibitors overcome suppressed cellular-mediated immunity by unleashing activated $CD8^+$ T-cell killing against tumor subsets [1]. Several commercially approved therapeutic antibodies have been reported to exhibit their tumor-killing effects through antibody-dependent cellular cytotoxicity (ADCC), antibody-dependent cellular phagocytosis (ADCP), and complement-dependent cytotoxicity (CDC) [2, 3]. The field encompassing these mechanisms is referred to as Humoral Immuno-Oncology (HIO). Translational findings have shown that tumors produce HIO factors that can suppress humoral immune pathways and in turn suppress the tumoricidal effects of ADCC, ADCP, and CDC [4–8]. Moreover, HIO factors can also bind to antibody

Abbreviations: ADC, antibody–drug conjugate; ADCC, antibody-dependent cellular cytotoxicity; CDC, complement-dependent cytotoxicity; HIO, humoral immuno-oncology; RTX, rituximab; TSTZ, trastuzumab.

components within antibody–drug conjugates (ADC), reduce their internalization and target cell killing [9].

The antibody-mediated humoral immune response is governed by antibody engagement with Fc-γ-activating receptors CD16a and CD32a on immune effector cells to initiate ADCC or ADCP as well as engage with C1q complement initiating protein to elicit antibody-bound target cell death via the classical CDC pathway [10].

Intercellular adhesion molecule 1 (ICAM-1) is a cell surface glycoprotein that is normally expressed on endothelial and immunocompetent cells. It is a member of the immunoglobulin superfamily and a transmembrane protein possessing an amino-terminus extracellular domain, a single transmembrane domain, and a carboxy-terminus cytoplasmic domain [11]. ICAM-1 is a ligand for LFA-1, a receptor found on leukocytes [12]. When activated, leukocytes bind to endothelial cells via ICAM-1/LFA-1 and then transmigrate into tissues [13]. It is also a ligand for tumor-expressed MUC1 [14]. The ICAM-1/MUC1 interaction is thought to support tumor metastasis in certain cancer types. Several reports have found that both tumor-produced soluble andmembrane-bound forms of ICAM-1 are associated with poor prognosis in patients with multiple myeloma (95%), NSCLC (75%), melanoma (70%), metastatic breast (63%), gastric (49%), metastatic colorectal cancers (40%), and large B cell lymphoma (28%), with the frequencies of expression for each cancer type shown in parentheses [15–17]. In particular, Roland et al. [16] report that the level of ICAM-1 expression on tumor cells dictates their metastatic potential and patient lethality. Additionally, several of these cancers are treated with antibody-based therapies employing immune effector mechanisms of killing, including trastuzumab and pertuzumab for breast cancer, cetuximab for colorectal cancer, rituximab for lymphoma, and daratumumab for multiple myeloma [6, 18–20].

In an attempt to identify the spectrum of tumor-produced HIO factors in human cancers, we have screened an array of proteins reported to be produced by various cancer types by employing molecular- and cell-based humoral immune response assays. As soluble ICAM-1 has been reported to be associated with a variety of cancers, we screened for its ability to suppress humoral immune activity via direct antibody binding and ADCC using cell-based reporter assays. Here, we report that both soluble and membrane-bound ICAM-1 proteins specifically interact with the CH3 domain of IgG1-type antibodies and in turn suppress their humoral immune activities (ADCC and CDC). Mutational analysis of IgG1 antibodies uncovered an essential motif within the CH3 domain required for ICAM-1 binding. Amino acid substitutions within this domain were found to render antibodies resistant to ICAM-1 binding and refractory to humoral immunosuppression. Moreover, ICAM-1 binding to antibody components of ADCs was found to reduce ADC target cell killing, similar to other HIO factor immunosuppressors [9]. This effect appears to involve ADC internalization, a requisite for maximal ADC target cell killing [21]. Here, we show that therapeutic antibodies in native and ADC formats could be engineered with a modified ICAM-1 binding domain to enable them to be more effective in killing cancer cells over expressing ICAM-1 or in microenvironments with soluble ICAM-1.

2 | Results

2.1 | Soluble ICAM-1 (sICAM-1) Binds to IgG1-Type Antibodies and Inhibits ADCC

Elevated ICAM-1 protein levels have been reported to be associated with various cancers as well as with poor prognosis of patients to standard-of-care therapies [15–17]. To evaluate its potential effect on humoral immunosuppression of antibody immune effector activity, sICAM-1 was first evaluated for antibody binding. Using ELISA assays, sICAM-1 or IgG1-type antibodies were coated on 96-well microplates and probed with biotinylated antibodies or sICAM-1, respectively. As shown in Figure 1A, biotinylated trastuzumab (TSTZ) is significantly bound to immobilized sICAM-1 but not to biotinylated control protein. Conversely, biotinylated sICAM-1 (b-sICAM-1) is significantly bound to immobilized pertuzumab (PTZ; Figure 1B) but not to immobilized control protein. To determine if ICAM-1 binding was specific for IgG1-type antibodies, other antibody isotypes were tested for sICAM-1 binding using similar assays as above. As shown in Figure S1, sICAM-1 appeared to be specific for binding IgG1 as no significant binding was observed with IgM, IgG2, or IgG4. ICAM-1 has been found to be expressed by endothelial and tumor cells in the hypoxic/acidic tumor microenvironment [22, 23]. ELISAs were conducted using acidic buffers to determine if ICAM-1 can bind IgG1 under acidic conditions. As shown in Figure S2B, ICAM-1 can significantly bind IgG1 in the acidic (pH 5.5) environment, showing its potential for humoral immunosuppression of antibodies targeting cells within the hypoxic/acidic microenvironment.

To evaluate if the binding of sICAM-1 could suppress antibody-mediated immune effector cell function, the Jurkat-CD16a ADCC reporter assay was employed as previously described [24]. CD20-expressing Daudi cells were used as target cells and treated with the anti-CD20 rituximab (RTX) antibody in the presence of varying sICAM-1 concentrations. As shown in Figure 1C, a significant dose-dependent inhibition of Jurkat-CD16a ADCC reporter cell activation was observed beginning at 1 μg/mL. To explore ICAM-1's broader activity against other therapeutic antibodies, cetuximab, TSTZ, and PTZ were tested against EGFR-positive A431 and HER-2-positive SK-BR-3 cells, respectively, using the same ADCC reporter assay format. As shown in Figure 1D, similar inhibitory results were observed, suggesting that sICAM-1 humoral immunosuppression was a universal phenomenon on IgG1-type antibodies. As sICAM-1 does not bind to CD16a Fc-γ-receptor (Figure S2A), we hypothesized that sICAM-1 binds directly to the antibody, thus mediating the observed sICAM-1 inhibition of CD16a effector function shown in Figure 1C,D. Next, we determined if sICAM-1 directly prevented the binding of antibodies to the ADCC activating CD16a Fc-γ-receptor via ELISA binding assays. As shown in Figure 1E, we observed a significant inhibition of CD16a binding to antibodies when substrate-bound cetuximab was probed with biotinylated CD16a in the presence of sICAM-1. Moreover, as CDC is a major mediator of humoral immunity for a number of commercially approved antibodies including cetuximab, RTX, and TSTZ, we investigated if sICAM-1 can also inhibit CDC. Under similar ELISA assay conditions and using biotinylated C1q

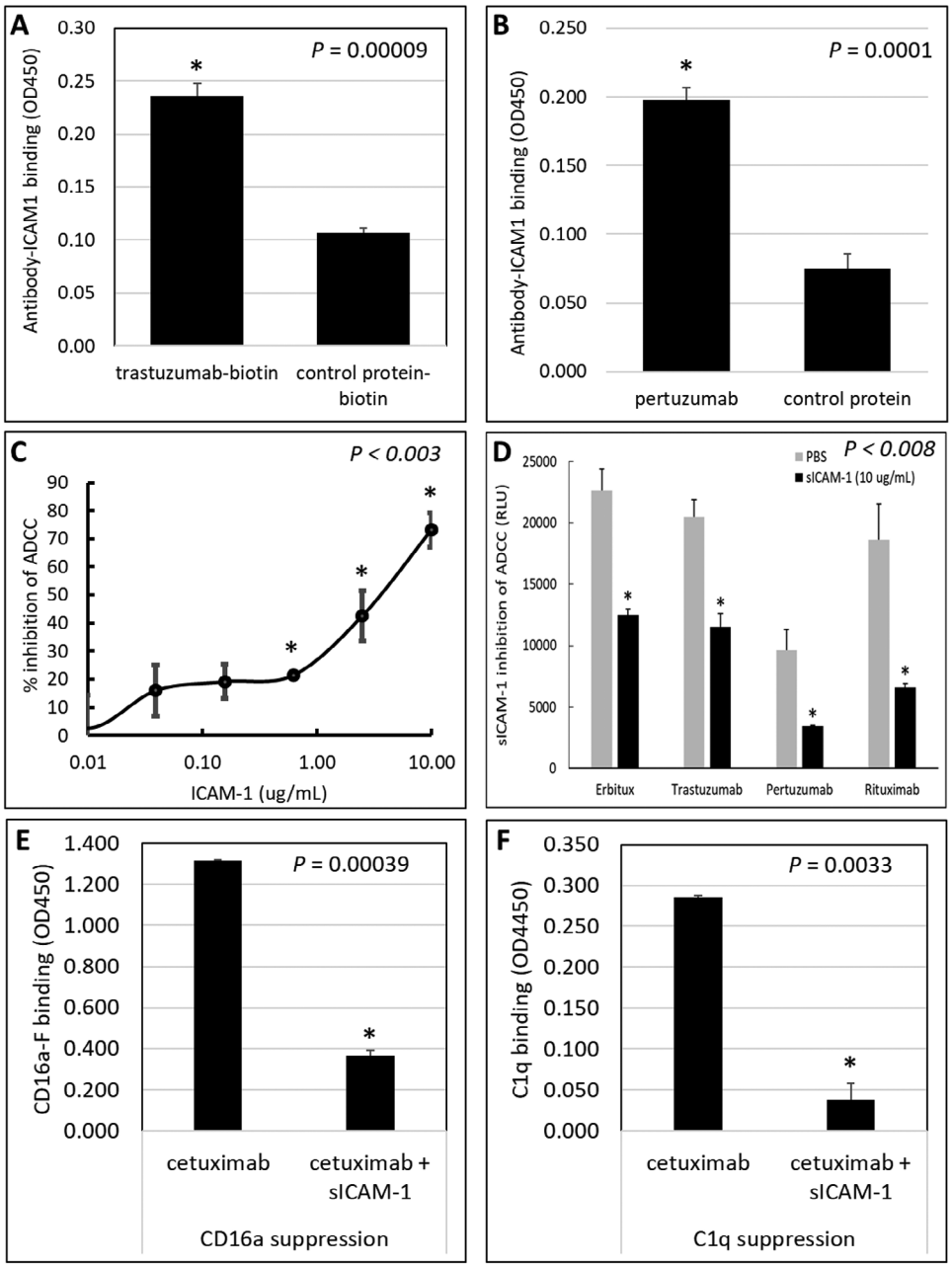

FIGURE 1 | Soluble ICAM-1 binds to IgG1-type antibodies and inhibits ADCC activity. (A) Substrate-bound soluble ICAM-1 (sICAM-1) was tested for binding to biotinylated TSTZ and irrelevant control protein human serum albumin (HSA). (B) Substrate-bound PTZ was tested for binding to biotinylated sICAM-1 and HSA control protein. Student's *t*-test was used to analyze the control protein signal to TSTZ and PTZ signal. Asterisks indicate statistically significant (p value <0.05) ADCC inhibition. (C) A dose titration of sICAM-1 on ADCC inhibition of RTX on Daudi target cells was tested using the Jurkat-CD16a ADCC reporter assay. Student's *t*-test was used to analyze signal of each concentration of sICAM-1 to no sICAM-1 control. (D) The effect of sICAM-1 on ADCC activity of pharmaceutically approved IgG1-type therapeutic mAbs was tested by comparing ADCC activity in the presence or absence of sICAM-1. The effect of sICAM-1 on cetuximab binding to CD16a Fc-γ-receptor (panel E) and C1q protein (panel F) was tested. Student's *t*-test was used to analyze the ADCC signal, CD16, or C1q binding of each antibody in the presence or absence of sICAM-1 in panels D, E, and F, respectively. All data points in panels are mean ± SD of triplicate values and are representative of three independent experiments.

as a probe, sICAM-1 was found to block C1q-IgG1 interaction (Figure 1F). Taken together, the presence of sICAM-1 in the tumor microenvironment could play a significant role in inhibiting the therapeutic activity of antibodies using immune effector activity. sICAM-1 binding assays testing antibody binding to target antigen found no effect on antibody-antigen binding.

2.2 | Soluble ICAM-1 Binds Within the Fc Domain of IgG1

An antibody fragmentation strategy was pursued in an attempt to identify the region to which ICAM-1 binds IgG1. First, IgG1-derived Fc and Fab fragments were generated via papain enzymatic digestion and used to coat ELISA plates in parallel with

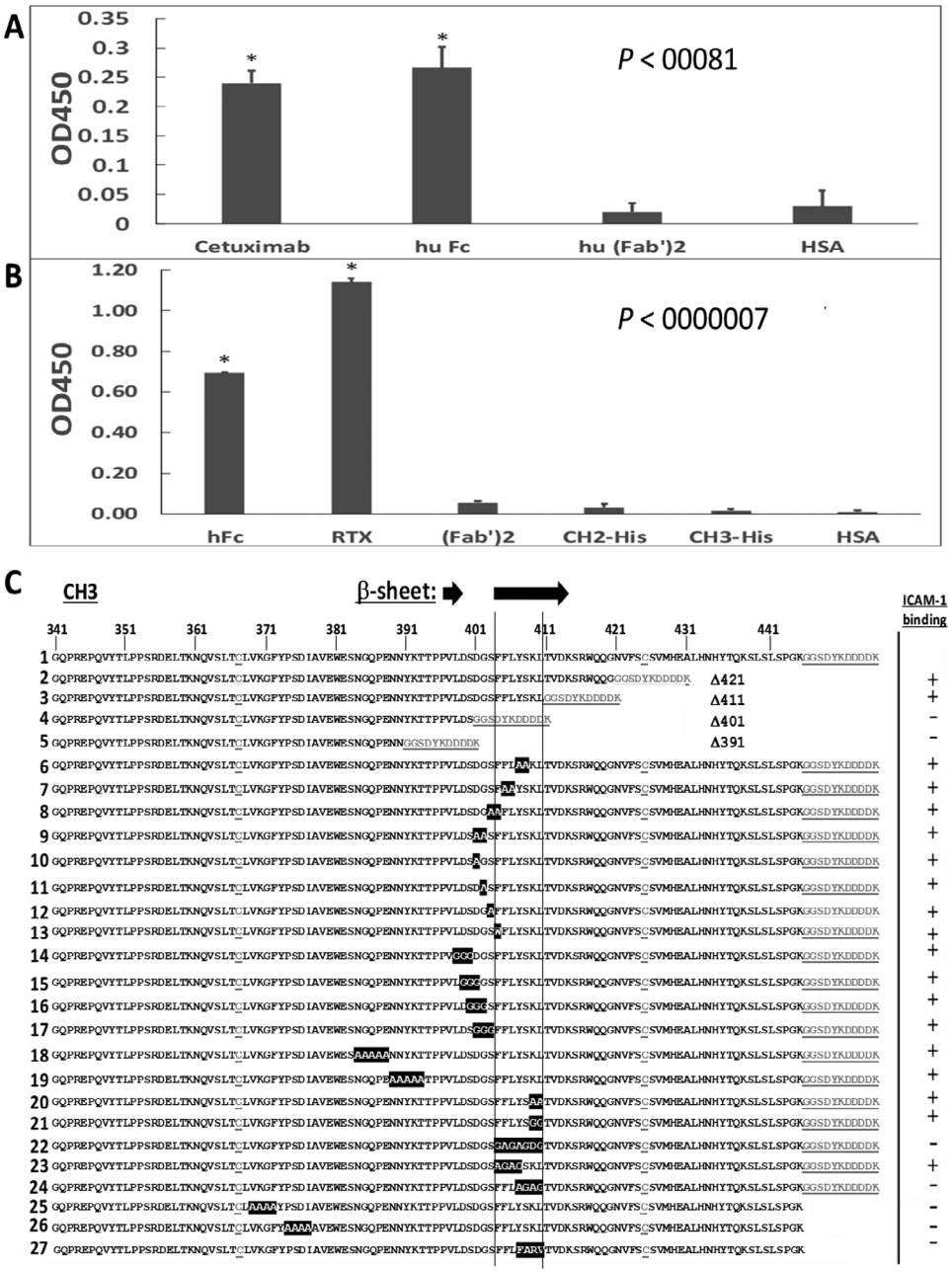

FIGURE 2 | sICAM-1 binds to the IgG1 Fc domain. (A) ELISAs using immobilized cetuximab and derived antibody fragments were tested for biotinylated sICAM-1 (b-sICAM-1) binding. (B) ELISAs using immobilized RTX, derived fragments, or recombinantly expressed CH domains were tested for b-sICAM-1 binding. For panels A and B, Student's *t*-test was used to individually analyze each sample binding signal compared with HSA signal. All data points in panels A and B are mean ± SD of triplicate values and are representative of three independent experiments. (C) IgG1 Fc mapping summary of the ICAM-1 binding domain constructs. Top numbering indicates residue position within the CH3 domain. The left column is construct numbers referred to in the Results section. Deletion constructs are designated with "Δ". Underlined grey amino acids indicate the Flag tag. Substitution mutations are highlighted in black. The right column indicates the ability (+) or inability (−) of antibody variants to bind ICAM-1. Vertical lines indicate the CH3 region of critical importance for ICAM-1 interaction. Loss of ICAM-1 binding to truncation mutations 4 and 5 but not 3 localizes the ICAM-1 binding region within the 404-410 amino acid sequence.

intact IgG1 (cetuximab). Plates were probed with biotinylated sICAM-1 (b-sICAM-1) and secondarily with streptavidin-HRP. As shown in Figure 2A, the Fc domain bound sICAM-1 similar to the full-length cetuximab, while $(Fab')_2$ control protein did not. In an effort to further define the binding region within the Fc domain, His-tagged single-chain CH2 and CH3 domains were recombinantly produced and tested via ELISA in parallel with proteolytically generated antibody fragments derived from the RTX antibody (Figure 2B). As observed above, full-length RTX and the papain-generated Fc domain bound sICAM-1, however, neither recombinant CH2 nor CH3 domain bound sICAM-1. These results suggested that either the bivalent interaction of

both heavy chain fragments was required for sICAM-1 binding or the binding domain included more than just the CH2 or CH3 domain. Strategies to address these possibilities were pursued below. The use of different full-length IgG1 antibodies, that is, cetuximab and RTX, were purposely employed to confirm a universal sICAM-1 binding domain within the IgG1 Fc structure.

2.3 | Mapping of the ICAM-1 Binding Domain by Deletion and Substitution Mutagenesis

To further delineate the IgG1 Fc ICAM-1 binding region, GST fusion proteins comprised of IgG1 N-terminal hinge through C-terminal CH3 region and a C-terminal Flag Tag were expressed in 293F cells to generate dimeric Fc fragments. We employed this strategy in light of the data above that showed sICAM-1 binding to IgG1 Fc dimer but not to single-chain CH2 or CH3 protein domains. Competition ELISAs employing supernatants from the various Fc constructs were used to identify those that may bind ICAM-1. Briefly, 96-well microplates were coated with RTX and then probed with b-sICAM-1 in the presence of the various construct supernatants. A summary of deletion constructs is shown in Figure 2C. An example of a typical competition assay is shown in Figure 3A, where b-sICAM-1 is shown in the left bar to bind the immobilized full-length IgG1 antibody. Bars to the right represent similar wells treated with potential competitor fragments. As shown, an excess of RTX antibody competed for sICAM-1 binding. As expected, GST-Fc (construct 1, Figure 2C) was also bound by sICAM-1, while $(Fab')_2$ and GST control did not. By using various deletion mutants in this assay, we were able to refine the sICAM-1 IgG1 binding domain. As shown in Figure 3A, construct 3, which deletes CH3 residues distal to amino acid 411, competed for sICAM-1 binding, while other deletion mutants within the CH3 domain (constructs 4 and 5) did not. These data suggest that the sICAM-1 binding region is localized in the dimeric IgG1 Fc CH3 domain. To further refine the residues essential for sICAM-1 CH3 binding, mutant full-length RTX antibodies were generated using glycine/alanine substitutions within the CH3 region. This approach was employed because systematic alanine substitution is useful in the identification of functional epitopes. The substitution removes all the side chain atoms past the beta-carbon. If any side chain function is present in the native protein, it is interfered with by the substitution of alanine as it lacks unusual backbone dihedral angle preferences. Additionally, glycine can also nullify the sidechain but adds a property of flexibility in the protein backbone [25]. Therefore, we used both residues to remove side chains as well as allow flexibility. As shown in Figure 3B, constructs 22 and 24 did not compete with sICAM-1 binding to parental RTX, while construct 21 showed partial competition. Because these residues appear hydrophobic, their effect on sICAM-1 binding may be a result of altered antibody tertiary structure. Further analysis of these constructs using functional assays to assess immune effector activity via ADCC reporter assays found all of them to be devoid of effector cell activation, suggesting that these amino acid changes caused a major perturbation of antibody Fc structure that negatively affects CD16a Fc-γ-receptor binding. Consistent with this view, previous reports have shown that CH3 tertiary structure is important for CH2 binding to Fc receptors as discussed below [26].

2.4 | ICAM-1 Affinity Binding to IgG1

As the binding of sICAM-1 appears specific for the IgG1 Fc domain, we determined its relative binding affinity using an ELISA-based competition assay. These assays have been previously shown to be reflective of relative protein-ligand binding affinity [27]. To validate the accuracy of this assay in comparison to surface plasmon resonance (SPR) methods, we tested the binding affinity of the low-affinity human CD16a Fc-γ-receptor (CD16a-158F) to IgG1. As shown in Figure S3A, the Ki inhibition constant was determined to be 683 nM, which is similar to the 720 nM affinity reported using SPR [28]. Using immobilized IgG1 and sICAM-1 as probes, we determined the Ki of sICAM-1 to IgG1 to be 288 nM (Figure S3B).

2.5 | Conservative Substitutions in the IgG1 407–410 Region Inhibits sICAM-1 Binding and Retains ADCC Activity

In an effort to generate CH3-modified IgG1 antibodies that are refractory to sICAM-1 binding and retain antibody immune effector function, additional modifications within the 407–410 region of RTX were performed by incorporating conservative amino acid substitutions [29, 30]. Modified full-length antibodies were then tested for sICAM-1 binding and ADCC activity. As shown in Figure 3C, parental RTX was able to block 79% of sICAM-1 interaction with substrate-bound RTX in the ELISA competition assay. Constructs 25, 26, and 27 exhibited less competitive ability (33%), inferring reduced ICAM-1 binding. For construct 27, we employed a point-accepted mutation scoring matrix (PAM250) [31]. In brief, this method suggested the most likely naturally occurring amino acid change at each given position as a way to conserve the buried domain, resulting in the YSKL to FARV amino acid sequence modifications. Variants were then tested for immune effector activity via ADCC reporter assays on Daudi target cells in the absence or presence of sICAM-1 (Figure 3D,E). While RTX mutants 25 and 26 did not have CD16a activation activity, RTX mutant 27 (referred to herein as RTX-FARV) showed robust CD16a activation in the presence of sICAM-1. Immunoprecipitation assays were performed with RTX and RTX-FARV to evaluate their interactions with sICAM-1. As shown in Figure S4A, a 75% reduction in ICAM-1 binding was observed using RTX-FARV compared with RTX (Figure S4B). Taken together, these data suggest the conservative FARV substitution of residues 407–410 within construct 27 retains robust ADCC activity while exhibiting a significant reduction of sICAM-1 binding and ADCC inhibition. Single amino acid changes within these residues had a lesser effect. Importantly, these four amino acid changes did not appear to change the overall biochemical properties of RTX-FARV compared with RTX as discussed below and shown in Figure S5.

2.6 | Membrane ICAM-1 Reduces IgG1 ADCC Activity and ADC Cytotoxicity

Previous research has shown that tumor-produced HIO factors that bind to ADCs may reduce their internalization and cytotoxicity against target cells [9]. Additionally, several reports have found that the soluble and membrane-bound ICAM-1 are elevated in a number of cancers [15, 17]. We, therefore, sought to determine

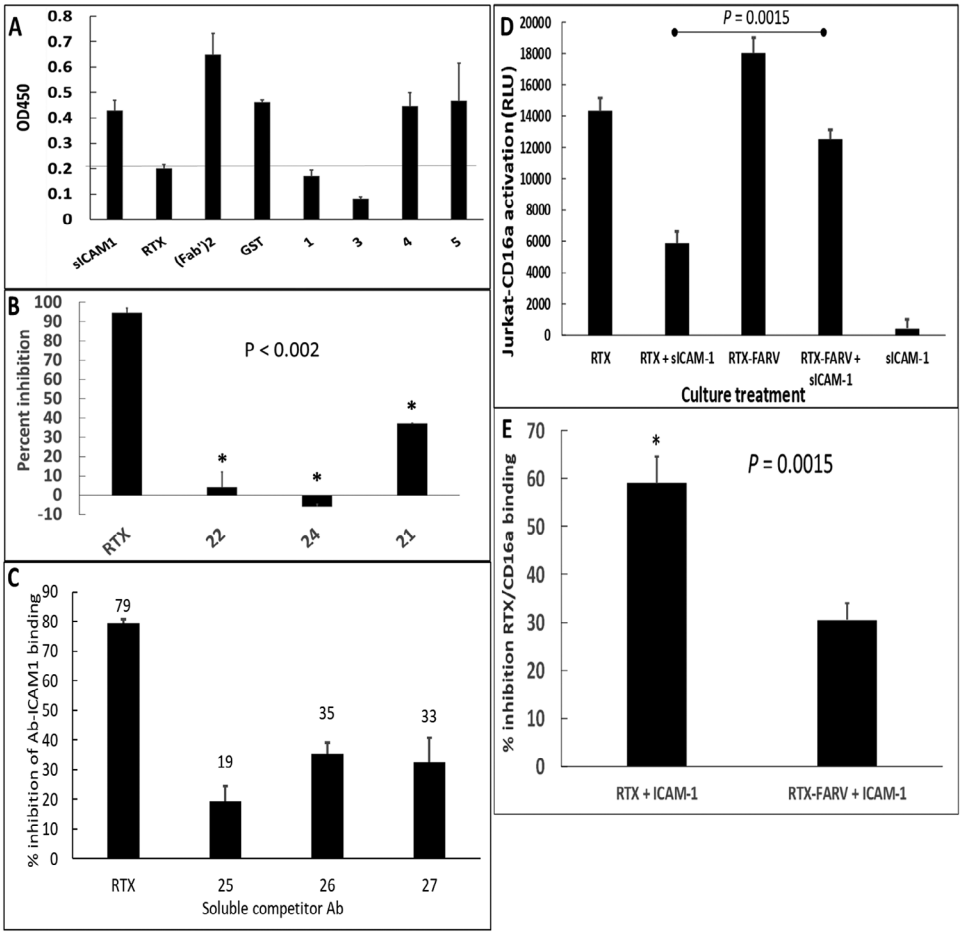

FIGURE 3 | Competition ELISAs map the ICAM-1 binding site within the IgG1 Fc CH3 domain. (A) Sample ELISA assay using deletion constructs. 96-well microplate plates coated with RTX were probed with b-ICAM-1 in the presence of supernatants containing various constructs at 5 μg/mL to test for competitive binding. Numbers indicate mutants from Figure 2C. A decrease in OD450 (below line) indicates competition via sICAM-1 binding to the soluble Fc competitor. (B) Quantified inhibition of sICAM-1 binding to gly-ala substitution mutations within the CH3 region 404–410. Numbers indicate mutants from summary data in Figure 2C. Student's *t*-test was used to individually analyze sICAM-1 binding inhibition to RTX by each mutant. (C) 96-well microplates were coated with RTX and probed with b-sICAM-1 in the presence of construct supernatants to determine sICAM-1 binding in the presence of mutant fragments. Percent inhibition is calculated as $1 - [(\text{competitor} + \text{b-ICAM-1})/(\text{no competitor} + \text{b-ICAM-1})] \times 100\%$. (D) To test the effect of sICAM-1 on RTX versus RTX-FARV ADCC suppression, Daudi cells were plated in triplicate wells with Jurkat-CD16 ADCC reporter cells and 100 ng/mL antibodies plus 5 μg/mL sICAM-1. RTX-FARV had significantly less ADCC inhibition by sCAM-1 compared with RTX ($p = 0.0015$). (E) Same as in panel D, where the % of inhibition of RTX/CD16 Fc receptor binding is shown. Student's *t*-test was used to compare inhibition of RTX to RTX-FARV in the presence of sICAM-1. All data points in panels are mean ± SD of triplicate values and are representative of three independent experiments.

in vitro if downregulation of membrane ICAM-1 expression in target cells would enhance the toxicity of ADCs containing wild-type IgG1 antibody components. To evaluate this, we employed anti-HER2 TSTZ and PTZ ADCs against HER2-expressing HCT-116 target cells modified with ICAM-1 shRNA constructs to silence ICAM-1 expression as previously described [24]. Multiple independent clones were generated and shown to have absent or reduced ICAM-1 protein expression (Figure 4A, top panel) while retaining similar amounts of HER2 target antigen expression as the parental line (Figure 4A, middle panel). Saporin-conjugated trastuzumab (TSTZ-ZAP) and pertuzumab (PTZ-ZAP) ADCs were tested on HCT-116 parental or isogenic HCT-116 shRNA ICAM-1 knockdown (HCT-116-KD) cells to determine if ICAM-1 affects ADC cytotoxicity. As shown in Figure 4B, both antibodies had a significant killing of HCT-116-KD cell clones 96.2 and 93.3 in comparison to parental (WT) and shRNA scrambled (SCRM) cell lines. To confirm the suppressive effects of ICAM-1 on TSTZ, we generated an ICAM-1 refractory TSTZ-FARV antibody and tested it for sICAM-1 immunosuppression using the Jurkat-CD16a ADCC assay. To avoid the potential effects of membrane ICAM-1, we used HCT-116 KD 93.3 cells as a target. Briefly, 96-well microplates were seeded with target cells and tested for CD16a activation using Jurkat-CD16a-158F (standard CD16a Fc low-affinity reporter cell employed in all other assays) and Jurkat-CD16a-158 V (CD16a Fc high-affinity reporter cell line) in the absence or presence of 5 μg/mL sICAM-1. As shown in Figure 4C, sICAM-1 significantly suppressed TSTZ CD16a activation in both reporter cell lines while no suppression was observed using TSTZ-FARV ($p < 0.0063$). These data suggest that membrane-bound ICAM-1 has an inhibitory role in ADC cytotoxicity and that membrane-bound ICAM-1 also has an immunosuppressive effect on TSTZ.

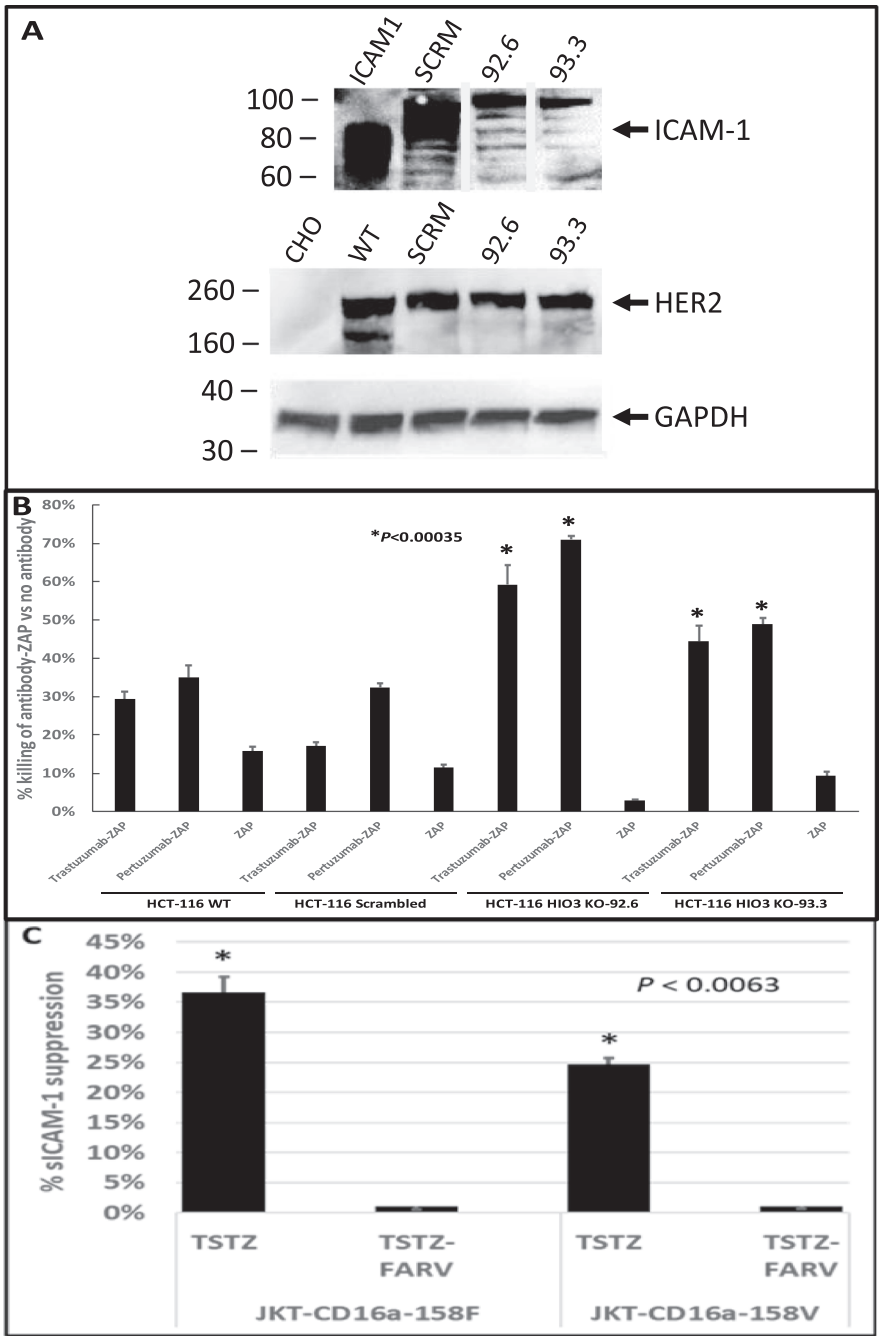

FIGURE 4 | Downregulation of ICAM-1 enhances antibody–drug conjugate (ADC) target cell killing. (A) Western blot analysis of ICAM-1 in HCT116 knockdown (KD) and scrambled (SCRM) cells. The top panel evaluates ICAM-1 expression from shRNA HCT116 SCRM, HCT116 KD 92.6, and 93.3 cells. ICAM-1 lane is sICAM-1 recombinant protein used as a positive control. Cell lysates were probed to confirm that equivalent HER2 expression was retained across the various cell lines. Lysates from Chinese Hamster Ovarian (CHO) cells were used as a HER2 negative control. The species cross-reactive anti-GAPDH antibody was used to show equivalent protein loading from the same lysates used for ICAM-1 and HER2 Westerns. Arrows indicate the expected molecular weight of each protein. Molecular weight values are indicated on the left side of each panel. Western blots are representative of two independent experiments. Full western blots for ICAM-1 and HER2 expression can be found in Figure S8. (B) ICAM-1 knockdown clones HCT-116 KD 92.6 and 93.3 were tested for antibody-saporin conjugate (ZAP) cytotoxicity as compared with the parental HCT-116 WT and scrambled control cell lines. Cytotoxicity of cells treated with TSTZ-ZAP, PTZ-ZAP conjugates, or saporin alone (ZAP) for 96 h was determined. Wells were stained with crystal violet to quantitate % cytotoxicity ((1-untreated cells/treated cells) × 100%). Student's *t*-test was used to compare ADC killing of HCT116 WT to HCT116 SCRM and HCT116 KD cell lines. (C) TSTZ-FARV was tested for sICAM-1 immunosuppression using Jurkat-CD16a-158F low affinity and Jurkat-CD16a-158 V high-affinity ADCC reporter cells. HCT-116 KD 93.3 cells were plated in 96-well microplates and tested for CD16a activation in the absence or presence of 5 μg/mL sICAM-1. sICAM-1 was able to suppress CD16a activation of parental TSTZ ($p < 0.0063$) while no suppression was observed using TSTZ-FARV. All data points in B and C are mean ± SD of triplicate values and are representative of three independent experiments. Significant killing is indicated by asterisks and determined using the student's *t*-test comparing the cytotoxicity of parental and FARV antibody mutants.

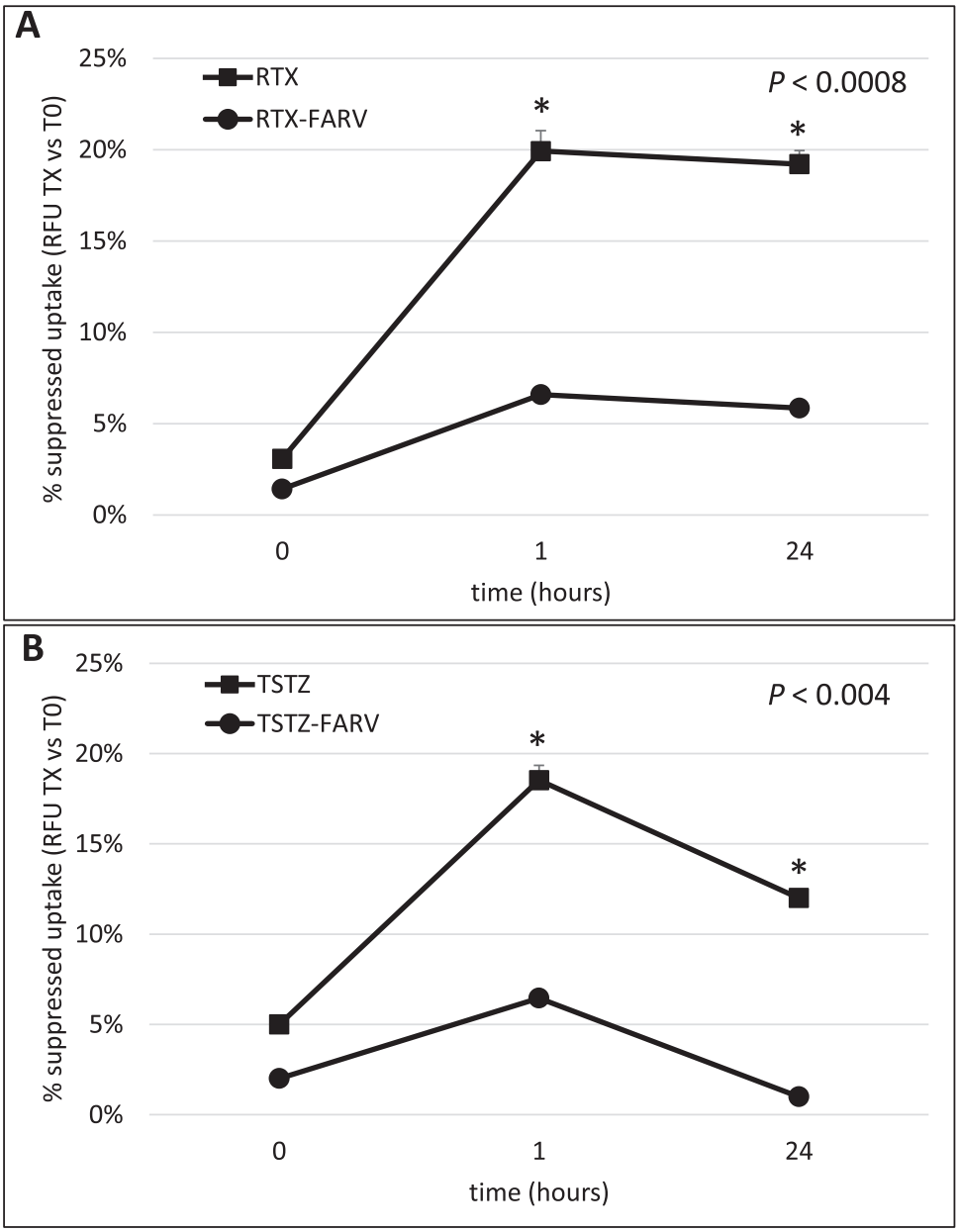

FIGURE 5 | IgG1 FARV mutants have enhanced internalization rates compared with parental antibodies in ICAM-1 expressing target cells. (A) OVCAR-CD20 cells were tested for internalization of RTX and RTX-FARV antibodies. Each antibody was converted into pHrodo probes and used to measure internalization from incubation time 0 (T0) to X (TX) for up to 24 h. RTX-FARV had significantly more internalization than parental RTX ($p < 0.0008$). (B) HCT116 cells were tested for internalization of parental TSTZ and TSTZ-FARV antibodies. TSTZ-FARV had significantly more internalization than TSTZ ($p < 0.004$). Percent internalization was determined by measuring relative fluorescence units (RFU) at various incubation time points vs T0. All data represent triplicate values. Student's *t*-test was used to compare parental and FARV antibodies at each timepoint. All data points in panels are mean ± SD of triplicate values and are representative of three independent experiments.

Previous studies have found that internalization rates are a key feature required for maximal ADC target cell killing [21] and that ADC interaction with cell surface proteins may inhibit uptake [9]. To determine if ICAM-1 binding to IgG1 may have an impact on antibody internalization, we employed the pHrodo internalization system to compare the internalization of RTX and RTX-FARV. As shown in Figure 5A, RTX had an approximately fourfold lower internalization than RTX-FARV ($p < 0.0008$) in OVCAR-CD20 target cells. To confirm the RTX findings, we also analyzed the internalization of TSTZ and TSTZ-FARV in HCT116 cells. As shown in Figure 5B, parental TSTZ had a ~10-fold lower internalization rate than TSTZ-FARV ($p < 0.004$). These data suggest that membrane-ICAM-1 negatively impacts IgG1 uptake and FARV-modified IgG1-based ADCs may benefit from improved target cell cytotoxicity when used to treat ICAM-1 expressing target cells.

One caveat of modifying residues within the IgG1 Fc domain may be the introduction of instable assembly or alterations of important physiological properties such as CD16a-Fc-γ-receptor binding for immune effector activity or FcRn binding, which is important for IgG1 systemic half-lives (Figure S7). To address

these potential issues, we have scaled both RTX-FARV and TSTZ-FARV production cell lines up to 200 mL cultures and found their homogeneity to be similar to that of their parental versions (Figure S5A). Binding analysis of CD16a Fc-γ-receptor to RTX-FARV appeared to be similar to parental RTX (Figure S5B), which is supportive of the ADCC findings shown in Figure 3D. Analysis of FcRn binding to RTX-FARV and TSTZ-FARV found both to be similar to their parental antibodies (Figure S5C). These findings support the potential use of FARV-modified IgG1-type antibodies to treat ICAM-1-expressing cancers.

3 | Discussion

Host humoral immune response mediated by antibodies eliciting cytotoxic effects against dysregulated cells is a powerful defense mechanism to eradicate transformed cells. Previous translational studies of antibodies used in cancer clinical trials have identified the CA125/MUC16 protein to immunosuppress humoral immune responses against antigen-expressing target cells [6, 8, 24]. In an attempt to identify other such proteins, we screened over 125 proteins reported in the literature to be expressed by tumors and present in the tumor microenvironment for direct IgG1 binding. Our efforts identified ICAM-1 as one of the very few proteins along with CA125 that bind IgG1 and, in turn, immunosuppress their immune effector activity. Interestingly, there appears to be a divergent overlap of ICAM-1 and CA125 in different cancer types. For example, over 95% of multiple myeloma express ICAM-1 with little to no CA125 overexpression [32, 33], while conversely, 95% of mesothelioma express CA125 with little to no ICAM-1 overexpression [8, 34].

Previous studies have shown that membrane-bound ICAM-1 plays a role in enhancing the ADCC of NK cells via LFA binding and blocking this interaction reduces its ADCC activity on target cells [35, 36]. Interestingly, none of these studies took into account the potential effect of ICAM-1 binding to antibodies. In order to avoid potential complications of the ICAM-1/LFA pathway on interpreting the effect of ICAM-1 on IgG1-mediated ADCC, we employed the Jurkat-CD16a reporter cell line that monitors CD16a Fc-γ-receptor activation independent of LFA, a prerequisite for ADCC activity by effector cells. As shown in Figure 1, sICAM-1 had a significant dose-response effect ($p < 0.003$) on suppressing RTX-mediated CD16a activation against Daudi cells (Figure 1C) as well as on other IgG1-type antibodies against antigen-expressing target cells ($p < 0.008$; Figure 1D). While human serum contains an abundance of IgG1, the impact of soluble and membrane ICAM-1 on therapeutic antibody immunosuppression is unknown. To address this, we employed the Jurkat-CD16a assay to measure the impact of human serum on TSTZ and the ICAM-1 refractory TSTZ-FARV. As shown in Figure S6A, TSTZ-FARV still showed a significantly better ADCC activation than the parental TSTZ, even in the presence of serum IgGs. These data suggest immune effector activity at the cell surface of the target cell may be negatively impacted by ICAM-1 despite the IgG1 levels in circulation.

Our findings show that ICAM-1 has specificity for the 407–410 CH3 domain of IgG1 but not IgG2, which is 100% identical to IgG1, or IgG4, which has a single amino acid change at 409. This may be likely due to distal amino acid changes that have been shown by others to affect antibody Fc three-dimensional structure and function [37].

The IgG1 CH3 domain is known to include the binding regions for various factors, including the neonatal Fc-receptor (FcRn), the tripartite motif-containing protein 21 (TRIM21), the Fc-receptor-like receptors (FcRL4/5), and *Staphylococcus* proteins A and G [38, 39]. This domain is also important for maintaining the tertiary structure of the Fc heavy chain, including residues located within the CH2 domain that are responsible for CD16a Fc-γ-receptor and C1q protein binding to elicit immune effector activities [26]. This is supported by our findings that certain nonconservative mutations within the ICAM-1 CH3 binding region can positively or negatively affect ADCC immune effector activity (Figure 2C). Interestingly, ICAM-1 binding appears to require CH3 in its dimeric form as CH3 monomers did not bind ICAM-1 in ELISA competition assays (Figure 2B) while Protein A and FcRn are reported to be able to bind to CH3 monomers. The crystal three-dimensional structure of the IgG1 CH3 domain has been found to be highly compacted in contrast to the CH2 domain, potentially explaining the need for dimeric CH3 structure to support ICAM-1 binding [40].

The finding that ICAM-1 binding to ADCs can negatively impact their target cell killing (Figure 4B) provides new insights and considerations for ADC engineering. First, it allows one to consider the appropriate use of ADCs in cancers that over express ICAM-1 for patient selection. Several cancers have been reported to over express ICAM-1 [16]. For approved ADCs used to treat ICAM-1-expressing cancer types, patients can first be screened to determine ICAM-1 status by immunohistochemistry or serum analysis for sICAM-1. Those with elevated ICAM-1 may not be ideal candidates for ADC treatment using antibody components with wild-type IgG1 CH3 residues. Alternatively, the use of ADCs containing IgG1 antibody components with a FARV motif may be useful in designing ADCs during the early development stage in addition to using optimal linkers and payloads. This concept is supported by the finding that RTX-FARV and TSTZ-FARV antibodies are less affected by ICAM-1 binding and diminished target cell internalization compared with parental RTX or TSTZ (Figure 5). Together, the molecular binding, ADCC, ICAM-1 cellular knockdown, and ADC killing data shown here confirm the inhibitory effects of ICAM-1 on IgG1-type antibody humoral immune effector activity due to direct antibody binding, and this effect may also negatively impact next-generation antibody formats such as ADCs.

4 | Materials and Methods

4.1 | Cell Lines and Growth Media

A431, Jurkat-CD16a, Daudi, HCT-116, HCT-116 shRNA clones, OVCAR-CD20, SKBR3, and HEK293F cells were all grown in RPMI 1640 with L-glutamine, penicillin/streptomycin, and 7.5% fetal bovine serum (R7.5). OVCAR-CD20 cells were grown in R7.5 containing 30 μg/mL blasticidin. HCT-116 shRNA clones were grown in R7.5 containing 1 μg/mL puromycin. Multiple independent HCT-116 shRNA ICAM-1 knockdown clones were generated using the shRNA constructs listed below that target

human ICAM-1 (Origene TG312270) (Sigma) in the same manner as previously described [24].

4.2 | Direct ELISA Antibody/sICAM-1 Binding Assays

Ninety-six-well ELISA microplates were coated with 2 μg/mL soluble human ICAM-1 (sICAM-1, Sino Biologicals), human IgG1-type antibodies, or control proteins in 50 mM carbonate, pH 9.0. For binding assays at pH 7.2, wells were washed with 0.05 M phosphate buffer pH 7.2 (PB7.2) and blocked for 1 h at room temperature with Pierce Blocking solution. Antibodies and sICAM-1 were biotinylated using the EZ-Link Sulfo-NHS-Biotin kit (ThermoScientific) and used as probes. Triplicate wells were probed with 10 μg/mL biotinylated antibodies or 1.5 μg/mL biotinylated sICAM-1 in PB7.2. Plates were washed with PB7.2 and secondarily probed with 50 ng/mL streptavidin-HRP in PB7.2 for 1 h. After washes with PB7.2, TMB colorimetric substrate was added for 5 min at room temperature followed by the addition of an equal volume of 0.1 N H_2SO_4 stop buffer. For binding assays at pH 5.5, similar methods were employed as above, with the exception of blocking with 5% milk, using 0.05 M PB pH5.5 (PB5.5). Binding was quantitated by absorbance at 450 nm on a Varioskan plate reader. All data points are mean ± standard deviation (SD) of triplicate values. Significance was determined using the Student's *t*-test.

4.3 | Jurkat CD16a-luciferase ADCC Reporter Assays

To test for sICAM-1 effects on ADCC, the Jurkat-CD16a-luciferase (Jurkat-CD16a) reporter cell assay (Promega) was employed as previously described [6, 8, 24]. For dose-dependent effects of sICAM-1 on ADCC, CD20-expressing Daudi cells were diluted to 3.64×10^5 cells/mL in ADCC assay buffer (RPMI + L-glutamine + 1% low Ig FBS) and seeded in black 96-well microplates in triplicate. Anti-CD20 RTX was added at a final concentration of 1 μg/mL with increasing concentrations of sICAM-1 up to 10 μg/mL. One hundred thousand Jurkat-CD16a cells were added and plates were incubated overnight at 37°C in 5% CO_2. Reporter cell activation was detected using Bio-Glo™ (Promega) luciferase substrate and lumens were quantified using a Varioskan plate reader. Percent inhibition by sICAM-1 was calculated by (1-lumens+sICAM-1/lumens-sICAM-1) × 100%. Using similar assays, a panel of commercially approved antibodies (cetuximab, TSTZ, PTZ) was screened using relevant antigen-specific target cell lines with 1 μg/mL antibodies and 10 μg/mL sICAM-1. SK-BR-3 cells were employed to test for sICAM-1 suppression on anti-HER2 TSTZ and PTZ antibodies. A431 cells were employed to test for suppression of the anti-EGFR cetuximab antibody. All data points are mean ± SD of triplicate values. Significance was determined by the student's *t*-test.

4.4 | FcRn Antibody Binding Assays

ELISA assays were used to assess CH3 mutations on FcRn-antibody binding. Soluble human FcRn (R&D Systems) was biotinylated using the EZ-Link Sulfo-NHS-Biotin kit (Thermo-Scientifc) and used as a probe. Ninety-six-well microplates were coated with 1 μg/mL of parental or CH3-modified antibodies in 50 mM carbonate, pH 9.0. Wells were washed with 0.05 M phosphate buffer, pH 7.2 (PB7.2), and blocked with PB pH 5.5 (PB5.5) plus 5% milk. Plates were then washed with PB5.5 and probed with 2.5 μg/mL biotinylated FcRn in PB5.5. Wells were washed and secondarily probed with 300 ng/mL streptavidin-HRP in PB5.5 plus 0.5% milk. Finally, wells were washed with PB5.5 and quantified using TMB colorimetric substrate, stopped, and analyzed as above. All data points are mean ± SD of triplicate values. Significance was determined using the student's *t*-test.

4.5 | CD16a and C1q Antibody Binding Assays

ELISA assays were employed to test for the impact of sICAM-1 on CD16a-antibody and C1q-antibody binding. Soluble human CD16a-158F-HIS (Sino Biologicals) and C1q (Sigma) proteins were biotinylated as above and used as probes. Ninety-six-well microplates were coated with 1 μg/mL of human IgG1-type antibody in 50 mM carbonate, pH 9.0. Wells were washed with 0.05 M phosphate buffer, pH 7.2 (PB), and blocked with PB plus 5% BSA. Plates were then washed and probed with 2.5 μg/mL biotinylated CD16a-158F-HIS or 1 μg/mL C1q with or without 10 μg/mL sICAM-1. Wells were washed and secondarily probed with 300 ng/mL streptavidin-HRP. Finally, wells were washed with PB and quantified using TMB colorimetric substrate, stopped, and quantified as above. All data points are mean ± SD of triplicate values. Significance was determined using the student's *t*-test.

4.6 | sICAM-1 Antibody Binding Competition Assays to Determine Affinity

ELISA competition assays were employed to determine the relative binding affinity of sICAM-1 to IgG1. Ninety-six-well microplates were coated with 1 μg/mL of IgG1-type antibody in 50 mM carbonate, pH 9.0. Wells were washed with 0.05 M phosphate buffer, pH 7.2 (PB), and blocked with PB plus 5% BSA. Plates were then washed and probed with 2.5 μg/mL biotinylated sICAM-1 in the presence of increasing amounts of nonlabelled sICAM-1 to determine a competition curve. Binding was detected using 300 ng/mL streptavidin-HRP. Values were plotted using a nonlinear regression analysis for 'saturation binding with one site' in GraphPad Prism version 9 (GraphPad Software, Inc.). As a control to evaluate the accuracy of this assay, biotinylated huCD16a-158F binding to IgG1 was evaluated using a similar method.

4.7 | Generation of Deletion and Substitution IgG1 Mutant Constructs

A fusion construct encoding an IgG1 secretion leader, human glutathione S transferase (GST), and human IgG1 constant region (from the N terminal hinge to C terminal CH3 region) and Flag Tag was synthesized (Integrated DNA Technologies). The fragment was PCR amplified using homologous primers containing 5'

*Hind*III and 3' *Eco*RI sequences (primers JBK0085,83; see primers list in the table below). The construct was subcloned into the pcDNA3 vector and sequenced to confirm construct integrity. Construct 1 showed the C-terminal region of this construct encoding the CH3 domain and Flag Tag. To generate secreted IgG1 CH2-His and CH3-His constructs, GST-Fc was used as a PCR template with primer sets JBK0038/48 and JBK0039/49, respectively to encode a secretion leader sequence and a C-terminal polyhistidine tag. Expression vector cloning was performed in a similar manner as above. Secreted constructs were purified with Ni-NTA resin (G Biosciences). C-terminal deletion constructs 2–5 were generated by PCR with primer JBK0085 in conjunction with 3' primers JBK0087-90, respectively. For substitution mutants (constructs 6–27), sense and antisense primers were synthesized to encode the highlighted mutations (Figure 2C). Primers were used with the QuickChange Lightning mutagenesis kit (Agilent). Individual clones were picked and integrity was confirmed by DNA sequencing before transient transfection into HEK-293F cells.

Primer	Sequence
JBK0085	TCCGCGGCCAAGCTTGCCGCCACCATGGAATGGAGCTGGGTGTTCCTGTTCTTTCTGT-CCGTGACCACAGGCGTGCATTCTATGCCGCCCTACACCGTG
JBK0083	AGGGAGAGGGGCGGAATTCTCACTTGTCGTCATCGTCTTTGTAGTCGCTGCCCCCTTT-CCCGGGAGACAGGGAGA
JBK0038	ACCGGCGTGCACAGCTCTTGTGACAAAACTCACACATGCCCACCGTGCCCAGCACCTG-AACTCCTGGGGGGACCG
JBK0039	ACCGGCGTGCACAGCTCTTGTGACAAAACTCACACATGCCCACCGTGCCCAGCACCTG-AACTCCTGGGGCAGCCCCGAGAACCACAGGTG
JBK0040	CCCAAGGACACCCTCATGATCTCCCGGACCCCTGAG
JBK0041	CTCAGGGGTCCGGGAGATCATGAGGGTGTCCTTGGG
JBK0087	AGGGAGAGGGGCGGAATTCTCACTTGTCGTCATCGTCTTTGTAGTCGCTGCCCCCCC-CCTGCTGCCACCTGCT
JBK0088	AGGGAGAGGGGCGGAATTCTCACTTGTCGTCATCGTCTTTGTAGTCGCTGCCCCCGA-GCTTGCTGTAGAGGAA
JBK0089	AGGGAGAGGGGCGGAATTCTCACTTGTCGTCATCGTCTTTGTAGTCGCTGCCCCCGG-AGTCCAGCACGGGAGG
JBK0090	AGGGAGAGGGGCGGAATTCTCACTTGTCGTCATCGTCTTTGTAGTCGCTGCCCCCGT-TGTTCTCCGGCTGCCC

4.8 | HEK-293F Transfection and Production of GST-Fc Fusions and Full-Length Antibody Mutants

To produce recombinant IgG1 Fc protein fragments, six-well plates were seeded with 2×10^5 HEK-293F cell/mL in R7.5 media overnight at 37°C in 5% CO_2. The following day, 2.5 μg of plasmids encoding GST-Fc fusion constructs or 1.25 μg of each heavy and light chain antibody constructs were transfected using lipofectamine 3000 (ThermoScientific). Cultures were grown for 120 h and supernatants were analyzed for recombinant protein production via dot blot. Positive expressing cultures were harvested and analyzed for integrity of recombinant protein size and homogeneity via Western blots. Blots analyzing antibody constructs were probed with anti-Fc-HRP (Jackson ImmunoResearch), while blots analyzing GST-Fc fusions were probed with anti-FlagTag-HRP antibody (Genscript).

4.9 | sICAM-1 Antibodies and Antibody Fragment Binding Assays

Ninety-six-well microplates were coated with 2.5 μg/mL of antibodies and fragments in triplicate in 50 mM carbonate, pH 9.0. Wells were then blocked with PBS plus 1% BSA and probed with 500 ng/mL of biotinylated sICAM-1 (b-sICAM-1) in PBS plus 1% BSA. Plates were washed with PBS plus 0.5% tween 20 (PBS-T) and secondarily probed with 300 ng/mL streptavidin-HRP. Finally, wells were washed with PBS-T followed by the addition of TMB colorimetric substrate, stopped, and quantified as above. All data points are mean ± SD of triplicate values. Significance was determined using the student's *t*-test.

4.10 | Coimmunoprecipitation of sICAM-1 with WT and Mutant Rituximab

Phosphate buffer (PB)-washed protein A agarose beads were aliquoted into 1.5 mL tubes with 2 μg of antibodies in 500 μL PB plus 2.5 μg ICAM-1-His or mesothelin-His (MLSN-His) used as negative control and rotated overnight at 4°C. Beads were pelleted, aspirated and washed twice with PB, then resuspended in Laemmli loading buffer with 2-mercaptoethanol and heated for 5 min at 95°C. Samples were electrophoresed on duplicate 4–12% bis-tris acrylamide gels and transferred to PVDF. Blots were blocked in 5% milk/PBS-T, then probed with 200 ng/mL of anti-His-HRP or anti-Fc-HRP (Genscript). Blots were washed with PBS-T and bands were visualized with SuperSignal West Femto

reagent (ThermoScientific) using an iBright Imaging System (InVitrogen).

4.11 | sICAM-1 GST-Fc Fusion and Fc Mutant Full-Length Antibody Competition Assays

Ninety-six-well microplates were coated with 2.5 μg/mL RTX in 50 mM carbonate, pH 9.0. Wells were blocked with PBS plus 1% BSA at room temperature then probed with 5 μg/mL of each fragment and 500 ng/mL biotinylated-sICAM-1 (b-sICAM-1). This concentration of b-sICAM-1 was chosen because it was 20-fold greater than the lowest detectable level of b-sICAM-1 by ELISA (23 ng/mL). Plates were then washed, secondarily probed with 300 ng/mL streptavidin-HRP, and quantified as described above. Percent inhibition was calculated as 1- [(competitor + b-sICAM-1)/ (no competitor + b-sICAM-1)] × 100%. Significance was determined using the student's *t*-test.

4.12 | RTX, RTX-FARV, TSTZ, and TSTZ-FARV ADCC Reporter Assays

To test the effects of CH3 amino acid changes on RTX ADCC, Daudi cells were resuspended at 9.09×10^5 cells/mL in ADCC assay buffer with 4×10^6 cells/mL of Jurkat-CD16a reporter cells. Daudi/Jurkat-CD16a cells (1×10^5 total cells) were seeded in opaque 96-well microplates in triplicate. To test the effects of CH3 amino acid changes on TSTZ ADCC, opaque 96-well microwell plates were seeded with 5.0×10^4 cells/mL in triplicate and grown overnight at 37°C in 5% CO_2. The next day, wells were washed and 1×10^5 cells/mL of Jurkat-CD16a cells in ADCC assay buffer was added. Antibodies were added at a final concentration of 100 ng/mL with or without 5 μg/mL sICAM-1. Plates were incubated at 37°C in 5% CO_2 for 6.5 h and quantified for Jurkat-CD16a activation via Bio-Glo luciferase substrate (Promega) on a Varioskan plate reader. Percent inhibition of ADCC activation by sICAM-1 was calculated by (1-lumens+sICAM-1/lumens-sICAM-1) × 100%. All data points are mean ± SD of triplicate values. Significance was determined using the student's *t*-test.

4.13 | Generation of Saporin Antibody–Drug Conjugates and Target Cell Killing Assays

Saporin ADCs were generated using the ZAP-Biotin Z system (Advanced Targeting Systems). First, TSTZ, PTZ, RTX, TSTZ-FARV, and RTX-FARV antibodies were biotinylated as described above. Equimolar amounts of biotinylated antibodies and streptavidin-linked-saporin (ZAP reagent) were then added and incubated at room temperature for 30 min to create antibody-ZAP ADCs. ZAP ADCs were then used directly in target cell-killing assays. To test for antibody-ZAP killing of target cells, HCT-116 wild type (WT), HCT-116-shRNA ICAM-1 knockdown (KD) clones, HCT-116-shRNA scrambled (SCRM) and/or OVCAR-CD20 cells were plated at 3,000 cells/well in clear 96-well microplates and grown overnight at 37°C in 5% CO_2. The next day, various amounts of ADCs (ranging from 100 nM to 1 fM) and controls were added to cells in triplicates, and plates were incubated for 96 h at 37°C in 5% CO_2. Wells were then washed in Ca^{++} and Mg^{++}-free PBS, and quantified via crystal violet staining as previously described [9]. Crystal violet-stained wells were solubilized with 1% SDS and quantified on a Varioskan plate reader at 570 nm. Percent cytotoxicity was calculated as (1-untreated cells/treated cells × 100%). All data points are mean ± SD of triplicate values. Significance was determined using the student's *t*-test.

4.14 | Antibody Internalization Assays

The pHrodo™ Red Avidin internalization assay (Invitrogen) was employed to monitor the cellular internalization of antibodies over a time course. Biotinylated RTX, RTX-FARV, TSTZ, TSTZ-FARV, and human IgM antibodies were used to generate pHrodo-labelled probes following the manufacturer's protocol. Briefly, equimolar amounts of biotinylated antibody and pHrodo red reagents were added in RPMI plus 1% BSA for 1 h on ice. After incubation, mixtures were centrifuged for 5 min at 12,000×*g* to remove aggregates and supernatants collected.

To prepare cells for pHrodo internalization analysis, opaque 96-well microplates were seeded with 1×10^5 OVCAR-CD20 cells to test RTX internalization or HCT116 cells to test for TSTZ internalization and grown overnight at 37°C in 5% CO_2 to allow cells to adhere to the well surface. The next day, plates were incubated on ice for 1 h, washed with ice-cold Ca^{++} and Mg^{++}-free PBS, and incubated with 10 μg/mL of each pHrodo-antibody suspended in ice-cold RPMI plus 1% BSA in triplicates. Plates were read for internalization by measuring pHrodo-pH sensitive dye fluorescence at 566/590 nM excitation/emission at various timepoints ranging from 1 min to 24 h of incubation at 37°C in 5% CO_2 using a Varioskan plate reader. Percent internalization was calculated by relative fluorescence unit (RFU) at each timepoint (TX)/fluorescence at T0. All data points are mean ± SD of triplicate values. Significance was determined using the student's *t*-test.

Author Contributions

Nicholas C. Nicolaide was the primary writer and contact of the manuscript, involved in developing, conceiving, and conducting experimental assays, and data interpretation. J. Bradford Kline edited the manuscript and was involved in developing, conceiving, and conducting experimental assays and data interpretation. Luigi Grasso conducted experimental assays and was involved in sample procurement, budgeting, and data interpretation.

Conflicts of Interest

The authors declare no conflicts of interest

Data Availability Statement

The data that support the findings of this study are available from the corresponding author upon reasonable request.

References

1. F. S. Hodi, S. J. O'Day, D. F. McDermott, et al., "Improved Survival With Ipilimumab in Patients With Metastatic Melanoma," *New England Journal of Medicine* 363 (2010): 711–723, https://doi.org/10.1056/nejmoa1003466.

2. D. J. Dilillo and J. V. Ravetch, "Fc-Receptor Interactions Regulate Both Cytotoxic and Immunomodulatory Therapeutic Antibody Effector Functions," *Cancer Immunology Research* 3 (2015): 704–713, https://doi.org/10.1158/2326-6066.CIR-15-0120.

3. T. Ruck, S. Bittner, H. Wiendl, and S. G. Meuth, "Alemtuzumab in Multiple Sclerosis: Mechanism of action and Beyond," *International Journal of Molecular Sciences* 16 (2015): 16414–16439, https://doi.org/10.3390/ijms160716414.

4. W. Wang, E. B. Somers, E. N. Ross, et al., "FCGR2A and FCGR3A Genotypes Correlate With Farletuzumab Response in Patients With First-Relapsed Ovarian Cancer Exhibiting Low CA125," *Cytogenetic and Genome Research* 152 (2017): 169–179, https://doi.org/10.1159/000481213.

5. J. B. Kline, S. Fernando, E. N. Ross, L. Grasso, and N. C. Nicolaides, "Tumor-Shed Antigen CA125 Blocks Complement-Mediated Killing Via Suppression of C1q-Antibody Binding," *European Journal of Immunology* 48 (2018): 1872–1882, https://doi.org/10.1002/eji.201847707.

6. L. Grasso, J. B. Kline, and N. C. Nicolaides, "Block-Removed Immunoglobulin Technology to Enhance Rituximab Effector Function by Counteracting CA125-Mediated Immunosuppression," *Oncology Letters* 23 (2022): 2, http://www.ncbi.nlm.nih.gov/pubmed/34820001, https://doi.org/10.3892/ol.2021.13120. Available at:. [Accessed September 10, 2023].

7. J. B. Kline, S. Fernando, S. Harley, L. Grasso, and N. C. Nicolaides, "Effect of CA125/MUC16 on Complement-Dependent Cytotoxicity (CDC) of Farletuzumab and Other CDC-Mediating Antibodies Via Inhibition of Antibody-C1q Binding," *Journal of Clinical Oncology* 35 (2017): e23082, https://doi.org/10.1200/jco.2017.35.15_suppl.e23082.

8. N. C. Nicolaides, C. Schweizer, E. B. Somers, et al., "CA125 Suppresses Amatuximab Immune-Effector Function and Elevated Serum Levels are Associated With Reduced Clinical Response in First Line Mesothelioma Patients," *Cancer Biology & Therapy* 19 (2018): 622–630, https://doi.org/10.1080/15384047.2018.1449614.

9. N. C. Nicolaides, J. B. Kline, and L. Grasso, "NAV-001, a High-Efficacy Antibody-Drug Conjugate Targeting Mesothelin with Improved Delivery of a Potent Payload by Counteracting MUC16/CA125 Inhibitory Effects," *PLoS ONE* 18 (2023): e0285161, https://doi.org/10.1371/journal.pone.0285161.

10. M. Reuschenbach, M. Von Knebel Doeberitz, and N. Wentzensen, "A Systematic Review of Humoral Immune Responses Against Tumor Antigens," *Cancer Immunology, Immunotherapy* 58 (2009): 1535–1544, https://doi.org/10.1007/S00262-009-0733-4.

11. J. Bella, P. R. Kolatkar, C. W. Marlor, J. M. Greve, and M. G. Rossmann, "The Structure of the Two Amino-Terminal Domains of Human ICAM-1 Suggests How It Functions as a Rhinovirus Receptor and as an LFA-1 Integrin Ligand," *PNAS* 95 (1998): 4140–4145, https://doi.org/10.1073/pnas.95.8.4140.

12. R. Rothlein, M. L. Dustin, S. D. Marlin, and T. A. Springer, "A Human Intercellular Adhesion Molecule (ICAM-1) Distinct from LFA-1," *The Journal of Immunology* 137 (1986): 1270–1274, https://doi.org/10.4049/jimmunol.137.4.1270.

13. L. Yang, R. M. Froio, T. E. Sciuto, A. M. Dvorak, R. Alon, and F. W. Luscinskas, "ICAM-1 Regulates Neutrophil Adhesion and Transcellular Migration of TNF-α-Activated Vascular Endothelium Under Flow," *Blood* 106 (2005): 584–592, https://doi.org/10.1182/blood-2004-12-4942.

14. T. Hayashi, T. Takahashi, S. Motoya, et al., "MUC1 Mucin Core Protein Binds to the Domain 1 of ICAM-1," *Digestion* 63 (2001): 87–92, https://doi.org/10.1159/000051917.

15. K. Hamazaki, A. Gochi, H. Shimamura, et al., "Serum Levels of Circulating Intercellular Adhesion Molecule 1 in Hepatocellular Carcinoma," *Hepato-Gastroenterology* 43 (1996): 229–234.

16. C. L. Roland, A. H. Harken, M. G. Sarr, and C. C. Barnett, "ICAM-1 Expression Determines Malignant Potential of Cancer," *Surgery* 141 (2007): 705–707, https://doi.org/10.1016/j.surg.2007.01.016.

17. M. Wu, X. Tong, D. Wang, L. Wang, and H. Fan, "Soluble Intercellular Cell Adhesion Molecule-1 in Lung Cancer: A Meta-analysis," *Pathology, Research and Practice* 216 (2020): 153029, https://doi.org/10.1016/j.prp.2020.153029.

18. B. Nami, H. Maadi, and Z. Wang, "Mechanisms Underlying the Action and Synergism Of Trastuzumab and Pertuzumab in Targeting HER2-Positive Breast Cancer," *Cancers (Basel)* 10 (2018): 342, https://doi.org/10.3390/cancers10100342.

19. D. J. Jonker, O. CJ, C. S. Karapetis, et al., "Cetuximab for the Treatment of Colorectal Cancer," *New England Journal of Medicine* 357 (2007): 2040–2048. A BS T R AC T.

20. T. Plesner and J. Krejcik, "Daratumumab for the Treatment of Multiple Myeloma," *Frontiers in Immunology* 9 (2018): 1228, https://doi.org/10.3389/fimmu.2018.01228.

21. F. Li, K. K. Emmerton, M. Jonas, et al., "Intracellular Released Payload Influences Potency and Bystander-Killing Effects of Antibody-Drug Conjugates in Preclinical Models," *Cancer Research* 76 (2016): 2710–2719, https://doi.org/10.1158/0008-5472.CAN-15-1795.

22. M. Soltani, M. Souri, and F. Moradi Kashkooli, "Effects of Hypoxia and Nanocarrier Size on pH-Responsive Nano-Delivery System to Solid Tumors," *Scientific Reports* 11 (2021): 19350, https://doi.org/10.1038/s41598-021-98638-w.

23. X. Liang, P. Arullampalam, Z. Yang, and X. F. Ming, "Hypoxia Enhances Endothelial Intercellular Adhesion Molecule 1 Protein Level through Upregulation Of Arginase Type II and Mitochondrial Oxidative Stress," *Front Physiol* 10 (2019): 1003, https://doi.org/10.3389/fphys.2019.01003.

24. J. B. Kline, R. P. Kennedy, E. Albone, et al., "Tumor Antigen CA125 Suppresses Antibody-Dependent Cellular Cytotoxicity (ADCC) Via Direct Antibody Binding and Suppressed Fc-γ Receptor Engagement," *Oncotarget* 8 (2017): 52045–52060, https://doi.org/10.18632/oncotarget.19090.

25. V. E. Gray, R. J. Hause, and D. M. Fowler, "Analysis of Large-Scale Mutagenesis Data to Assess the Impact of Single Amino acid Substitutions," *Genetics* 207 (2017): 53–61, https://doi.org/10.1534/genetics.117.300064.

26. E. O. Saphire, R. L. Stanfield, M. D. Max Crispin, et al., "Contrasting IgG Structures Reveal Extreme Asymmetry and Flexibility," *Journal of Molecular Biology* 319 (2002): 9–18, https://doi.org/10.1016/S0022-2836(02)00244-9.

27. M. Syedbasha, J. Linnik, D. Santer, et al., "An ELISA Based Binding and Competition Method to Rapidly Determine Ligand-receptor Interactions," *Journal of Visualized Experiments* no. 109 (2016): 53575, https://doi.org/10.3791/53575-v.

28. P. Li, N. Jiang, S. Nagarajan, R. Wohlhueter, P. Selvaraj, and C. Zhu, "Affinity and Kinetic Analysis of Fcγ Receptor IIIa (CD16a) Binding to IgG Ligands," *Journal of Biological Chemistry* 282 (2007): 6210–6221, https://doi.org/10.1074/jbc.M609064200.

29. W. R. Pearson, "Selecting the Right Similarity-Scoring Matrix," *CP in Bioinformatics* 43 (2013): 3.5.1–3.5.9, https://doi.org/10.1002/0471250953.bi0305s43.

30. S. French and B. Robson, "What is a Conservative Substitution?," *Journal of Molecular Evolution* 19 (1983): 171–175, https://doi.org/10.1007/BF02300754.

31. M. O. Dayhoff, R. M. Schwartz, and B. C. Orcutt, *Atlas of Protein Sequence and Structure* (Washington, D.C.: National Biomedical Research Foundation, 1978).

32. M. Boota, C. Schinke, S. Ledoux, D. Alapat, R. Khan, and B. Barlogie, "CA-125 Secreting IgG Kappa Multiple Myeloma," *American Journal of Hematology* 91 (2016): E457–E458, https://doi.org/10.1002/ajh.24456.

33. D. W. Sherbenou, Y. Su, C. R. Behrens, et al., "Potent Activity of an Anti-ICAM1 Antibody-Drug Conjugate Against Multiple Myeloma,"

Clinical Cancer Research 26 (2020): 6028–6038, https://doi.org/10.1158/1078-0432.CCR-20-0400.

34. G. Alì, N. Borrelli, G. Riccardo, et al., "Differential Expression of Extracellular Matrix Constituents And Cell Adhesion Molecules between Malignant Pleural Mesothelioma and Mesothelial Hyperplasia," *Journal of Thoracic Oncology* 8 (2013): 1389–1395, https://doi.org/10.1097/JTO.0b013e3182a59f45.

35. S. Cooley, L. J. Burns, T. Repka, and J. S. Miller, "Natural Killer Cell Cytotoxicity Of Breast Cancer Targets is Enhanced by Two Distinct Mechanisms of Antibody-Dependent Cellular Cytotoxicity Against LFA-3 and HER2/neu," *Experimental Hematology* 27 (1999): 1533–1541, https://doi.org/10.1016/S0301-472X(99)00089-2.

36. D. Sanchez-Martinez, N. Allende-Vega, S. Orecchioni, et al., "Expansion of Allogeneic NK Cells with Efficient Antibody-Dependent Cell Cytotoxicity Against Multiple Tumors," *Theranostics* 8 (2018): 3856–3869, https://doi.org/10.7150/thno.25149.

37. G. Vidarsson, G. Dekkers, and T. Rispens, "IgG Subclasses and Allotypes: From Structure to Effector Functions," *Frontiers in Immunology* 5 (2014): 520, https://doi.org/10.3389/fimmu.2014.00520.

38. S. W. de Taeye, T. Rispens, and G. Vidarsson, "The Ligands for Human IgG and Their Effector Functions," *Antibodies* 8 (2019): 30, https://doi.org/10.3390/antib8020030.

39. T. Ying, W. Chen, Y. Feng, Y. Wang, R. Gong, and D. S. Dimitrov, "Engineered Soluble Monomeric IgG1 CH3 Domain Generation, Mechanisms of Function, and Implications for Design of Biological Therapeutics," *Journal of Biological Chemistry* 288 (2013): 25154–25164, https://doi.org/10.1074/jbc.M113.484154.

40. J. Deisenhofer, "Crystallographic Refinement and Atomic Models of a Human Fc fragment and its Complex with Fragment B of Protein A from *Staphylococcus aureus* at 2.9- and 2.8-Å Resolution," *Biochemistry* 20 (1981): 2361–2370, https://doi.org/10.1021/bi00512a001.

Supporting Information

Additional supporting information can be found online in the Supporting Information section.